


RESEARCH ARTICLE

Robust output regulation of a triaxial MEMS gyroscope via nonlinear active disturbance rejection

Mehran Hosseini-Pishrobat | Jafar Keighobadi 

Faculty of Mechanical Engineering,
University of Tabriz, Tabriz, Iran

Correspondence

Jafar Keighobadi, Faculty of Mechanical
Engineering, University of Tabriz, Tabriz
51666 14766, Iran.
Email: Keighobadi@tabrizu.ac.ir

Summary

This paper presents a nonlinear disturbance rejection-based controller for the robust output regulation of a triaxial microelectromechanical system (MEMS) vibratory gyroscope. In a MEMS gyroscope, parameter variations, mechanical couplings, suspension system nonlinearities, thermal noise, and centripetal/Coriolis forces are the main uncertainty sources. In the dynamical equations of the gyroscope, these uncertainties appear as a matched total disturbance, which does not coincide with the required structure of a standard output regulation problem. More specifically, the total disturbance is not guaranteed to belong to the solution space of a fixed dynamical system. Therefore, we propose a control system that comprises a nominal output regulator equipped with a disturbance rejection loop. On the basis of a suitable reference dynamics of the gyroscope, the control system is developed as the stabilization of a zero-error invariant manifold in the tracking error space. In the disturbance rejection loop, a nonlinear extended state observer (ESO) is designed to estimate the total disturbance. The convergence of the ESO is analyzed in a Lyapunov-Lurie framework by linear matrix inequalities (LMIs). In the nominal output regulation loop, the stabilization problem of the desired manifold is tackled by introducing a suitable distance coordinate. Next, to achieve guaranteed attenuation of the ESO estimation errors, an energy-to-peak design is pursued. On the basis of the center manifold theory, the stability of the overall closed-loop system is guaranteed. The efficacy of the proposed control method is assessed through software simulations.

KEYWORDS

disturbance rejection, extended state observer, output regulation, triaxial MEMS gyroscope

1 | INTRODUCTION

Microelectromechanical system (MEMS) gyroscopes are one of the most widely used MEMS sensors in the emerging fields of applications where angular velocity measurement is required. For example, a triple set of MEMS gyroscopes and accelerometers forms a complete inertial measurement unit for navigation and guidance purposes.¹⁻³ The advent of MEMS gyroscopes had a great impact on the development of vehicular control systems used for improving safety and comfort in driving.³ The other fields of applications include robotics, consumer electronics, virtual reality, and military.^{1,2,4}

Current micromachining technologies allow the batch fabrication of the silicon MEMS gyroscopes with low per-device cost.⁴ Compact size, low energy consumption, and the capability of integration with electronics for signal processing/control are the striking features that create a great opportunity for these sensors to replace the conventional macro-sized gyroscopes.^{1,2} However, the miniaturized size of a MEMS gyroscope imposes limiting effects on its performance. The operation of MEMS devices is sensitive to geometric and structural defects caused by the inevitable imperfections of fabrication techniques.^{1,2} Besides, environmental factors such as temperature affect the physical properties of the constituent material and perturb the sensor dynamics by random noise.^{2,4} Therefore, to realize a robust MEMS gyroscope, various closed-loop control techniques have been proposed in recent literature. Park and Horowitz⁶ proposed an adaptive controller to estimate online all parameters of the gyroscope through a parameter adaptation loop. Then, the estimated parameters were used to compensate for the mechanical couplings and Coriolis forces by a feedforward control law. Zheng et al⁷ proposed an active disturbance rejection controller for MEMS gyroscope applications and tested the method experimentally on a piezoelectrically actuated vibrating beam gyroscope. In our previous work,⁸ a model predictive control system was proposed for the force-balancing operation mode of a vibratory gyroscope considering the saturation of control inputs.

In recent years, triaxial MEMS gyroscopes capable of angular rate detection about 3 independent axes have gained much attention as a major thrust in the development of microfabricated inertial sensors.⁹ Using a single mass to realize the vibratory gyroscope offers promising advantages such as reduction in footprint size, improved productivity, and attenuation of mechanical interferences ubiquitous for systems of multiple masses.¹⁰ John and Vinay¹⁰ proposed a new device concept that has a single oscillating mass with actuation and sensing components along 3 orthogonal axes. Both position and velocity of the mass are resolved by the sensing elements and are then fed back to an adaptive vibration controller. Fei and Zhou¹¹ designed a robust model reference controller for a triaxial gyroscope using sliding-mode techniques. An adaptive fuzzy system was used to compensate for the uncertainty and the disturbances in a Lyapunov-based framework. Song et al¹² designed an adaptive dynamic surface controller for the triaxial gyroscope considering dead-zone and input saturation nonlinearities. The control method uses fuzzy logic for uncertainty approximation.

Active disturbance rejection control (ADRC) is a robust control method that actively estimates and then compensates for the discrepancy between the underlying physical system and its nominal mathematical model.¹³ In this regard, uncertainties, noise, and external disturbances are all lumped in a *total disturbance* term.¹³ The dynamical model of the underlying system is extended through considering the total disturbance as a fictitious state variable.^{13,14} Next, an extended state observer (ESO) is used to estimate the extended state vector.¹⁵ The estimated total disturbance is used to reject the total disturbance, so that the physical system converges to the nominal model. As a salient feature, the ADRC does not rely on accurate modeling of the system and, hence, can handle large uncertainties and external disturbances.¹⁴ The reader could refer to the works of Han¹³ and Huang and Xue¹⁴ and the references therein for more details on the ADRC systems and their applications.

The basic problem of the output regulation theory is in achieving asymptotic tracking and/or disturbance rejection for a class of signals generated by an autonomous dynamical system.¹⁶⁻¹⁸ The general framework for tackling this problem is to convert the output regulation problem into a stabilization problem of an auxiliary system.^{16,18} To this end, the steady-state trajectory of a given plant is considered to match the reference signal. Considering the difference between the plant trajectory and the desired steady-state response, one can apply feedforward control for output regulation. However, the feedforward method is highly model dependent and sensitive to uncertainties/perturbations.¹⁸ The internal model principle, as a prominent tool of the output regulation theory, enables the design of structurally robust regulators capable of dealing with model uncertainty and perturbations.¹⁶⁻¹⁸ Such regulators use a dynamic compensator, known as the internal model, to transform the output regulation problem of the plant into a stabilization problem. Internal model-based output regulation techniques have been developed and studied in a wide variety of applications such as adaptive attitude tracking of a rigid spacecraft subjected to disturbances with unbounded energy,^{19,20} adaptive output regulation of torsional electrostatic micromirrors with geometric constraints,²¹ and robust attitude control of helicopters and autonomous flight vehicles.^{17,22} The vibration control problem of a MEMS gyroscope, in essence, includes the tracking of reference signals with known frequencies. Accordingly, the MEMS gyroscope control problem can be formulated and handled through standard tools of the output regulation theory. This point of view, however, has not been considered in the existing control techniques for MEMS gyroscopes.

The main contribution of this paper is in solving the robust vibration control problem of a triaxial MEMS gyroscope by combining the output regulation theory with the disturbance rejection control. The discrepancy between the nominal and physical gyroscope systems, including parametric uncertainty, nonlinear stiffness terms, thermal noise, and centripetal/Coriolis forces, is represented by a total disturbance. We formulate the tracking control problem of the gyroscope

as the stabilization of an invariant manifold. Unlike a conventional output regulation problem, the total disturbance does not belong to the solution space of a fixed dynamical system. Thereby, to handle the total disturbance, we add a disturbance rejection loop to the nominal output regulation. To this end, a nonlinear ESO is designed to estimate the total disturbance. A linear matrix inequality (LMI) framework is developed to establish the ESO convergence using a Lyapunov-Lurie function. For the nominal output regulation, we propose an internal model-based framework to render the target manifold attractive. Through integrating the estimated total disturbance with the nominal control law, the gyroscope system trajectories converge practically to the manifold. In comparison with the related control techniques, the following novelties are presented.

1. In the conventional ADRC, the nominal controller is designed by the feedforward control of a suitable error dynamics.^{7,14} From the output regulation perspective, this method is sensitive to the perturbations of a nominal system (see the work of Chen and Huang¹⁸ for more details). As a result, the control system is rendered vulnerable to the estimation errors of the disturbance rejection loop. To remedy this issue, we propose a more robust nominal output regulator by using the internal model principle. The obtained nominal regulator rejects those components of the disturbance estimation errors with the same frequency spectrum as the reference signals. Moreover, to achieve guaranteed attenuation of the disturbance estimation errors, we apply the energy-to-peak robust control.
2. The reported control methods of triaxial MEMS gyroscopes, cited in this paper, assume that both the position and velocity vectors of the proof mass are available. Owing to the technical difficulties and high cost, the position measurement is mostly available for the control system of a practical gyroscope.⁴ Therefore, in all design steps of the control system, we only require the position vector of the proof mass. We also address the issue of measurement noise using the ESO with nonlinear gains.

The rest of this paper is organized as follows. In Section 2, mathematical modeling of a triaxial MEMS gyroscope is explained. The control problem is formulated in Section 3. In Section 4, an ESO is designed for disturbance rejection. The nominal output regulation is elaborated in Section 5. The closed-loop stability is analyzed in Section 6. Software simulations are performed in Section 7 to verify the effectiveness of the proposed method. Finally, concluding remarks are presented in Section 8.

2 | DESCRIPTION OF MEMS GYROSCOPE SYSTEM

The mechanical model of a triaxial MEMS gyroscope is approximated as a 3-degree-of-freedom system comprised of a vibrating proof mass suspended by the stiffness and damping components (see Figure 1). To investigate the dynamics of the gyroscope, first, a ground-fixed inertial reference frame $I = (E_1, E_2, E_3)$ is introduced. Next, a non-inertial reference frame $\tilde{I} = (\tilde{E}_1, \tilde{E}_2, \tilde{E}_3)$ is considered, which is rigidly attached to the sensor's framework participating in its motion. The origin of the reference frame \tilde{I} , point \mathcal{O} , coincides with the neutral position of the proof mass. It is assumed that the

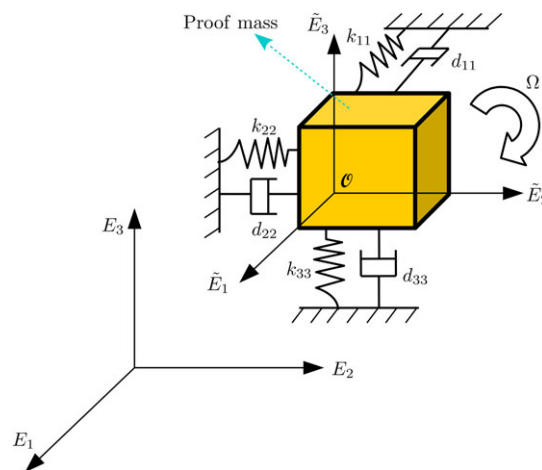


FIGURE 1 Mechanical model of a triaxial microelectromechanical system gyroscope [Colour figure can be viewed at wileyonlinelibrary.com]

acceleration of point \mathcal{O} with respect to the inertial frame is negligible. In a typical working condition of the sensor, the gyroscope frame $\tilde{\mathcal{I}}$ is subjected to an angular velocity $\Omega : \mathbb{R}^+ \rightarrow \mathbb{R}^3$, with respect to the inertial reference frame \mathcal{I} . The coordinates of Ω with respect to $\tilde{\mathcal{I}}$ are given as $\Omega = [\Omega_1, \Omega_2, \Omega_3]^\top$. Regarding the proof mass element of the gyroscope as a point mass m , the mechanical configuration of the system is specified by the position components q_1 , q_2 , and q_3 along the \tilde{E}_1 , \tilde{E}_2 , and \tilde{E}_3 axes, respectively. Hence, we use $q := [q_1, q_2, q_3]^\top \in \mathbb{R}^3$ as the vector of generalized coordinates and $\dot{q} := [\dot{q}_1, \dot{q}_2, \dot{q}_3]^\top \in \mathbb{R}^3$ as the vector of generalized velocities in the description of the gyroscope dynamics. Applying the Euler-Lagrange equation, we obtain the equation of motion as follows:

$$M\ddot{q} + D\dot{q} + Kq + \Phi(q) = u + C(q, \dot{q}, t), \quad (1)$$

where

- $u := [u_1, u_2, u_3]^\top \in \mathbb{R}^3$ denotes the control force applied through the electrostatic actuators;
- $M = mI \in \mathbb{R}^{3 \times 3}$ is the inertia matrix;
- $D = D^\top = [d_{ij}] \in \mathbb{R}^{3 \times 3}$ is the damping matrix representing the viscous effects of the ambient atmosphere and the internal friction of the constituent material^{4,23};
- $K = K^\top = [k_{ij}] \in \mathbb{R}^{3 \times 3}$ is the linear stiffness matrix, and $\Phi(q) = [\alpha_1 q_1^3, \alpha_2 q_2^3, \alpha_3 q_3^3]^\top \in \mathbb{R}^3$ accounts for the nonlinear behavior of the microbeams caused by midplane stretching²³;
- $C(q, \dot{q}, t) = 2mS(\Omega)\dot{q} - m(\dot{S}(\Omega) + S^2(\Omega))q$ groups the centripetal and Coriolis forces, with $S(\Omega) \in \mathbb{R}^{3 \times 3}$ being a skew symmetric matrix associated with the angular velocity vector, ie,

$$S(\Omega) = \begin{bmatrix} 0 & \Omega_3 & -\Omega_2 \\ -\Omega_3 & 0 & \Omega_1 \\ \Omega_2 & -\Omega_1 & 0 \end{bmatrix}.$$

To put the gyroscope dynamics (1) in a controller design perspective, we introduce the following considerations C1, C2, and C3.

- C1: Owing to the fabrication imperfections and variations of the environmental factors, only nominal values of the stiffness and damping parameters are available. More specifically, $K = K_n + \delta K$ and $D = D_n + \delta D$, where K_n and D_n stand for the nominal values and δK and δD represent the bounded variations. The nonlinear stiffness parameters α_i are assumed to be unknown.
- C2: As a result of thermal agitation of the gas molecules surrounding the sensor, a mechanical-thermal noise force disturbs the gyroscope dynamics.²⁴ We consider the mechanical-thermal noise as a bounded input disturbance $\tau : \mathbb{R}^+ \rightarrow \mathbb{R}^3$.
- C3: The generalized coordinates q_i are the measured outputs of the gyroscope. In practice, capacitive detectors are used to resolve the proof mass's position along the gyroscope frame axes.^{4,23} The output signal is contaminated by electrical-thermal measurement noise, caused by the agitation of electrons in the sensing circuit.²⁵ The noise enters the measurement equation as a bounded additive perturbation $\vartheta : \mathbb{R}^+ \rightarrow \mathbb{R}^3$, where $\|\vartheta(\cdot)\|_{\mathcal{L}_\infty} \leq \vartheta_0$.

Owing to the diversified scales of the gyroscope parameters, the equation of motion (1) is nondimensionalized. Setting m , q_0 , and w_0 , respectively, as the reference mass, length, and frequency, we introduce the following normalized variables:

$$\frac{q}{q_0} \rightarrow q, \quad \frac{K}{mw_0^2} \rightarrow K, \quad \frac{\alpha_i q_0^2}{mw_0^2} \rightarrow \alpha_i, \quad \frac{D}{mw_0} \rightarrow D, \quad \frac{S(\Omega)}{w_0} \rightarrow S(\Omega), \quad \frac{u}{mq_0 w_0^2} \rightarrow u, \quad \frac{\tau}{mq_0 w_0^2} \rightarrow \tau, \quad \frac{\vartheta}{q_0} \rightarrow \vartheta.$$

On the basis of the aforementioned considerations, the dynamical equation of the gyroscope (1) is rewritten in the following form:

$$\ddot{q} + D_n \dot{q} + K_n q = u + \Delta(q, \dot{q}, t), \quad (2)$$

where $\Delta : \mathbb{R}^3 \times \mathbb{R}^3 \times \mathbb{R}^+ \rightarrow \mathbb{R}^3$ is the total disturbance caused by the parametric uncertainty, nonlinearities, and external disturbances, ie,

$$\Delta(q, \dot{q}, t) = -\delta K q - \delta D \dot{q} + \Phi(q) + C(q, \dot{q}, t) + \tau(t).$$

3 | FORMULATION OF THE CONTROL PROBLEM

The basic task of a gyroscope control system is to properly shape the mechanical energy of the sensor, while compensating for parameter variations, mechanical couplings, nonlinearities, and thermal/electrical noise.⁵ In this regard, the vibration

amplitudes and frequencies of the gyroscope axes should be regulated to some fixed values to attain the required energy level. From the control design perspective, this amounts to regulating the proof mass's trajectory to the signals generated by a reference model of the gyroscope. In general, the reference model is governed by a differential equation of the form

$$\ddot{q}_m + K_m q_m = 0, \quad (3)$$

where $q_m \in \mathbb{R}^3$ is the reference generalized coordinate vector and $K_m \in \mathbb{R}^{3 \times 3}$ is a positive-definite diagonal matrix that determines the reference vibration frequencies. The initial conditions of system (3) range over an admissible subset of the corresponding state space.

Remark 1. The specifications of the reference dynamical model depend on the operation mode of the sensor. For example, in the adaptively controlled gyroscope proposed in the work of John and Vinay,¹⁰ the reference dynamics generates a 3-dimensional Lissajous trajectory. The obtained reference signal guarantees a consistent adaptation of the controller parameters by satisfying the required level of persistence excitation.

To pose the control problem in a standard output regulation framework, we first consider the so-called regulator equations.^{17,18} These equations correspond to the steady-state output of the gyroscope that perfectly tracks the reference signal. That is,

$$\begin{aligned} q_s &= q_m, \\ \dot{q}_s &= \dot{q}_m, \\ u_s &= \ddot{q}_m + D_n \dot{q}_m + K_n q_m - \Delta_s(q_m, \dot{q}_m, t), \end{aligned} \quad (4)$$

where $q_s \in \mathbb{R}^3$ denotes the steady-state generalized coordinates, $u_s \in \mathbb{R}^3$ is the steady-state control force of output regulation, and $\Delta_s(q_m, \dot{q}_m, t) \in \mathbb{R}^3$ is the associated value of the total disturbance. The solvability of the regulator equations is instrumental in solving the associated output regulation problem.¹⁸ For a given reference signal $q_m(\cdot)$, the equations always admit a unique solution for the steady-state generalized coordinates q_s and velocities \dot{q}_s . The required control u_s contains the Coriolis force and the mechanical-thermal disturbance, which depend on the working and environmental conditions of the sensor. Therefore, in general, u_s is not uniquely determined by $q_m(\cdot)$ but it also depends on the particular working condition of the gyroscope. Nevertheless, the existence of a steady-state output regulation control force is always guaranteed. The tracking performance of the control system is quantified by the error variable

$$e := q - q_m. \quad (5)$$

Accordingly, we introduce the following composite system consisting of the physical (2) and the reference (3) gyroscope systems

$$\Sigma_c : \begin{cases} \ddot{q} + D_n \dot{q} + K_n q = u + \Delta(q, \dot{q}, t), \\ \ddot{q}_m + K_m q_m = 0. \end{cases} \quad (6)$$

From a geometrical point of view, the regulator equations describe an output zeroing, controlled invariant manifold for Σ_c defined as¹⁸

$$\mathcal{M} := \{ \text{col}(q, \dot{q}, q_m, \dot{q}_m) \in \mathbb{R}^{12} \mid q - q_m = 0, \dot{q} - \dot{q}_m = 0 \}. \quad (7)$$

In the state space of Σ_c , under the control input u_s , if the system motion initiates on \mathcal{M} , the trajectories will evolve on \mathcal{M} for all times $t \in \mathbb{R}^+$, and the tracking error will be identically equal to zero. From this perspective, a global output regulation of the MEMS gyroscope amounts to rendering the manifold \mathcal{M} attractive. In other words, the control system should regulate the gyroscope trajectories to those of the regulator equations. The steady-state control input u_s is composed of a unique nominal part defined as $u_s^n := \ddot{q}_m + D_n \dot{q}_m + K_n q_m$ and an uncertain part $\Delta_s(q_m, \dot{q}_m, t)$. By the reference dynamical equation (3), the nominal steady-state control u_s^n admits a differential equation of the form $\ddot{u}_s^n + K_m u_s^n = 0$. This differential equation, usually referred to as the steady-state generator, implies the existence of an internal model.^{16,18} However, owing to the nonlinearities and disturbances, the uncertain term $\Delta_s(q_m, \dot{q}_m, t)$ does not conform to any dynamic structure and, hence, cannot be compensated by the internal model approach. On the basis of this argument, we propose a disturbance rejection-based control method to tackle the robust output regulation problem of the gyroscope. Following a 2-degree-of-freedom configuration, the control system is composed of a nominal output regulator equipped with an active disturbance rejection loop. The nominal regulator produces the required control force for the output regulation of the following nominal gyroscope system;

$$\ddot{q} + D_n \dot{q} + K_n q = u_n. \quad (8)$$

In this regard, the nominal regulator recovers u_s^n by driving the nominal closed-loop trajectories toward the target manifold \mathcal{M} . Moreover, the active disturbance rejection loop reconstructs $\Delta_s(q_m, \dot{q}_m, t)$ by estimating online the total disturbance. The overall control law is composed of 2 terms, that is,

$$u(t) = u_n(t) - \hat{\Delta}(t), \quad (9)$$

with $\hat{\Delta}(\cdot)$ being an estimate of the total disturbance signal. We study the robustness of the nominal regulator against the disturbance estimation errors in Section 5. It should be noted that the active disturbance rejection loop can be interpreted as an approximate output regulation technique.²⁶ That is, since the steady-state total disturbance does not conform to a dynamic generator, it is modeled and compensated by an approximate dynamics. We expand on this point of view in Section 4.

4 | ESO DESIGN

Considering $x_1 = q$, $x_2 = \dot{q}$, and $x_3 = \Delta(q, \dot{q}, t)$, the equation of motion (2) is represented by the following extended state equations:

$$\begin{aligned} \dot{x}_1 &= x_2, \\ \dot{x}_2 &= -K_n x_1 - D_n x_2 + x_3 + u, \\ \dot{x}_3 &= h(t), \\ y &= x_1 + \vartheta(t), \end{aligned} \quad (10)$$

in which y is the measurement vector, $\vartheta(\cdot)$ is the measurement noise, and

$$h(t) := \frac{d}{dt} \Delta(q, \dot{q}, t) = \frac{\partial}{\partial q} \Delta(q, \dot{q}, t) \dot{q} + \frac{\partial}{\partial \dot{q}} \Delta(q, \dot{q}, t) \ddot{q} + \frac{\partial}{\partial t} \Delta(q, \dot{q}, t).$$

The physical limits and mechanical structure of a MEMS gyroscope do not allow rapid unbounded changes in the velocity and acceleration of the proof mass.⁷ The disturbance term $\Delta(q, \dot{q}, t)$ is a polynomial function of q and \dot{q} , and hence, the associated partial derivatives are well defined and bounded. In a normal working condition of the sensor, the angular velocity and acceleration are bounded functions of time. Taking this point together with consideration C2, the boundedness of the partial derivative of the total disturbance with respect to time $\partial \Delta(q, \dot{q}, t) / \partial t$ is inferred. On the basis of this reasoning, the signal $h(\cdot)$ is considered to be bounded, that is, $\|h(\cdot)\|_{\mathcal{L}_\infty} \leq h_0$.

In the framework of a high-gain design, we propose the following observer to reconstruct the total disturbance:

$$\begin{aligned} \dot{\hat{x}}_1 &= \hat{x}_2 + \frac{H_1}{\varepsilon} g_1(y - \hat{x}_1), \\ \dot{\hat{x}}_2 &= -K_n \hat{x}_1 - D_n \hat{x}_2 + \hat{x}_3 + u + \frac{H_2}{\varepsilon^2} g_2(y - \hat{x}_1), \\ \dot{\hat{x}}_3 &= \frac{H_3}{\varepsilon^3} g_3(y - \hat{x}_1), \end{aligned} \quad (11)$$

where \hat{x}_i stands for the estimate of x_i , $H_i \in \mathbb{R}^{3 \times 3}$ are the design matrices, and $\varepsilon > 0$ is the high-gain parameter of the observer. The observer innovation process is defined by the nonlinear functions $g_i : \mathbb{R}^3 \rightarrow \mathbb{R}^3$, with $g_i(0) = 0$. To ensure the existence and uniqueness of the solutions of the system (11), we assume that $g_i(\cdot)$ are locally Lipschitz continuous.

Remark 2. From the point of view of output regulation theory, the extended state equation $\dot{x}_3 = h(t)$ is an approximate dynamical model characterizing the containing set of $\Delta(\cdot)$ rather than its exact trajectory. The corresponding estimation law of \hat{x}_3 can be regarded as an integrator-type internal model.²⁶ Accordingly, the ESO (11) can be conceived as an approximate output regulation method.

To investigate the convergence of the proposed ESO, using the error variables $\tilde{x}_i := x_i - \hat{x}_i$, we obtain the following estimation error dynamics:

$$\begin{aligned} \dot{\tilde{x}}_1 &= -\frac{H_1}{\varepsilon} (\tilde{x}_1 + \vartheta(t)) + \tilde{x}_2 + \frac{H_1}{\varepsilon} \phi_1(\tilde{x}_1 + \vartheta(t)), \\ \dot{\tilde{x}}_2 &= -\frac{H_2}{\varepsilon^2} (\tilde{x}_1 + \vartheta(t)) - K_n \tilde{x}_1 - D_n \tilde{x}_2 + \tilde{x}_3 + \frac{H_2}{\varepsilon^2} \phi_2(\tilde{x}_1 + \vartheta(t)), \\ \dot{\tilde{x}}_3 &= -\frac{H_3}{\varepsilon^3} (\tilde{x}_1 + \vartheta(t)) + \frac{H_3}{\varepsilon^3} \phi_3(\tilde{x}_1 + \vartheta(t)) + h(t), \end{aligned} \quad (12)$$

where $\varphi_i(z) := z - g_i(z)$ for all $z \in \mathbb{R}^3$. The parameter ε is typically a small positive constant that results in fast time domain characteristics for the solutions of Equation 12. Accordingly, we consider the following coordinate transformation²⁷:

$$\eta_i = \varepsilon^{i-1} \tilde{x}_i, i = 1, 2, 3. \quad (13)$$

By setting $\eta := \text{col}(\eta_1, \eta_2, \eta_3)$ and $\zeta := \eta_1$, the error dynamics (12) is transformed into the following singularly perturbed system:

$$\begin{aligned} \varepsilon \dot{\eta} &= A_0(\varepsilon)\eta + \sum_{i=1}^3 F_i \phi_i(\zeta + \vartheta(t)) + Q_\vartheta \vartheta(t) + \varepsilon^3 Q_h h(t), \\ \zeta &= C_0 \eta. \end{aligned} \quad (14)$$

The system matrices are given by

$$\begin{aligned} A_0(\varepsilon) &= \begin{bmatrix} -H_1 & I & O \\ -H_2 - \varepsilon^2 K_n & -\varepsilon D_n & I \\ -H_3 & O & O \end{bmatrix}, F_1 = \begin{bmatrix} H_1 \\ O \\ O \end{bmatrix}, F_2 = \begin{bmatrix} O \\ H_2 \\ O \end{bmatrix}, F_3 = \begin{bmatrix} O \\ O \\ H_3 \end{bmatrix}, \\ Q_\vartheta &= \begin{bmatrix} -H_1 \\ -H_2 \\ -H_3 \end{bmatrix}, Q_h = \begin{bmatrix} O \\ O \\ I \end{bmatrix}, C_0 = [I \ O \ O]. \end{aligned}$$

The commonly used linear high-gain ESOs suffer from the amplification of the measurement noise.²⁷ To remedy this issue, various nonlinear gains have been designed and discussed in the literature.^{15,27} On the basis of the nonlinear observer in the work of Ball and Khalil,²⁷ we use the following decentralized gain functions with design parameters $0 < \sigma < 1$ and $d > 0$:

$$\begin{aligned} g_i(z) &= [g_{i1}(z_1) \ g_{i2}(z_2) \ g_{i3}(z_3)]^\top, i = 1, 2, 3; \\ g_{ij}(z_j) &= \begin{cases} \sigma^i z_j, & |z_j| \leq d \\ z_j + d(\sigma^i - 1)\text{sgn}(z_j), & |z_j| > d \end{cases}, j = 1, 2, 3. \end{aligned} \quad (15)$$

By incorporating a dead-zone-type nonlinearity to automatically adjust the observer gain, the functions in Equation 15 achieve robustness against noise. When the estimation error falls into the zone $[-d, d]$, the observer gain decreases to prevent noise amplification.

Assumption 1. The nominal ESO error dynamics defined as

$$\begin{aligned} \varepsilon \dot{\eta} &= A_0(\varepsilon)\eta + \sum_{i=1}^3 F_i \phi_i(\zeta) \\ \zeta &= C_0 \eta \end{aligned} \quad (16)$$

has a globally exponentially stable equilibrium at the origin.

Theorem 1. Under Assumption 1, the solutions of the ESO error dynamics (12) are globally bounded and globally ultimately bounded. More specifically, after a finite transient time t_0 , the practical convergence of the ESO is achieved in the sense that

$$\|x_i - \hat{x}_i\| \leq \rho_i + \mu_\vartheta \frac{\vartheta_0}{\varepsilon^{i-1}} + \varepsilon^{4-i} \mu_h h_0, i = 1, 2, 3, \quad (17)$$

for all $t \geq t_0$, some positive numbers μ_ϑ , μ_h , and arbitrarily small $\rho_i > 0$.

Proof. The state equation (14) is rewritten as

$$\varepsilon \dot{\eta} = A_0(\varepsilon)\eta + \sum_{i=1}^3 F_i \phi_i(\zeta) + \sum_{i=1}^3 F_i [\phi_i(\zeta + \vartheta(t)) - \phi_i(\zeta)] + Q_\vartheta \vartheta(t) + \varepsilon^3 Q_h h(t). \quad (18)$$

Owing to Assumption 1, there is a positive-definite function $V(\eta)$ satisfying

$$\lambda_1 \|\eta\|^2 \leq V(\eta) \leq \lambda_2 \|\eta\|^2, \left\| \frac{\partial V}{\partial \eta} \right\| \leq \lambda_3 \|\eta\|, \left. \frac{dV(\eta)}{dt} \right|_{(16)} \leq -\frac{\lambda_4}{\varepsilon} \|\eta\|^2,$$

for some positive constants $\lambda_1, \lambda_2, \lambda_3$, and λ_4 .²⁸ By calculating the time derivative of $V(\eta)$ along the solutions of Equation 18, we obtain

$$\begin{aligned} \left. \frac{dV(\eta)}{dt} \right|_{(18)} &= \left. \frac{dV(\eta)}{dt} \right|_{(16)} + \frac{1}{\varepsilon} \frac{\partial V}{\partial \eta} \left(\sum_{i=1}^3 F_i(\phi_i(\zeta + \vartheta(t)) - \phi_i(\zeta)) + Q_\vartheta \vartheta(t) + \varepsilon^3 Q_h h(t) \right) \\ &\leq -\frac{\lambda_4}{\varepsilon \lambda_2} V(\eta) + \frac{1}{\varepsilon} (\mu_0 \vartheta_0 + \varepsilon^3 \mu_1 h_0) \sqrt{V(\eta)}, \end{aligned} \quad (19)$$

where $\mu_0 := \lambda_3 (\sum_{i=1}^3 \|F_i\| (1 - \sigma^i) + \|Q_\vartheta\|) / \sqrt{\lambda_1}$ and $\mu_1 := \lambda_3 \|Q_h\| / \sqrt{\lambda_1}$. Dividing both sides of Equation 19 by $2\sqrt{V(\eta)}$ and using the comparison lemma,²⁹ we obtain

$$\sqrt{V(t)} \leq \exp\left(-\frac{\lambda_4 t}{2\varepsilon \lambda_2}\right) \sqrt{V(0)} + \frac{\lambda_2}{\lambda_4} (\mu_0 \vartheta_0 + \varepsilon^3 \mu_1 h_0) \left(1 - \exp\left(-\frac{\lambda_4 t}{2\varepsilon \lambda_2}\right)\right).$$

Therefore, we have

$$\|\eta(t)\| \leq \sqrt{\frac{\lambda_2}{\lambda_1}} \exp\left(-\frac{\lambda_4 t}{2\varepsilon \lambda_2}\right) \|\eta(0)\| + \frac{\lambda_2}{\lambda_4 \sqrt{\lambda_1}} (\mu_0 \vartheta_0 + \varepsilon^3 \mu_1 h_0) \left(1 - \exp\left(-\frac{\lambda_4 t}{2\varepsilon \lambda_2}\right)\right). \quad (20)$$

By switching to the primary error coordinates \hat{x}_i for $i = 1, 2, 3$, we obtain the following inequalities from Equation 20, which clearly show the boundedness of the estimation error:

$$\|\tilde{x}_i(t)\| \leq \varepsilon^{1-i} \sqrt{\frac{\lambda_2}{\lambda_1}} \exp\left(-\frac{\lambda_4 t}{2\varepsilon \lambda_2}\right) \|\eta(0)\| + \frac{\lambda_2 \varepsilon^{1-i}}{\lambda_4 \sqrt{\lambda_1}} (\mu_0 \vartheta_0 + \varepsilon^3 \mu_1 h_0) \left(1 - \exp\left(-\frac{\lambda_4 t}{2\varepsilon \lambda_2}\right)\right). \quad (21)$$

For a given positive ρ_i , we define a time t_i as

$$t_i := \frac{2\varepsilon \lambda_2}{\lambda_4} \log \left(\frac{\left| \sqrt{\frac{\lambda_2}{\lambda_1}} \|\eta(0)\| - \frac{\lambda_2}{\lambda_4 \sqrt{\lambda_1}} \frac{(\mu_0 \vartheta_0 + \varepsilon^3 \mu_1 h_0)}{\varepsilon^{i-1}} \right|}{\rho_i \varepsilon^{i-1}} \right).$$

The ultimate bounds in the inequality (17) hold with $t_0 = \max\{t_1, t_2, t_3\}$, $\mu_\vartheta = \lambda_2 \mu_0 / \lambda_4 \sqrt{\lambda_1}$ and $\mu_h = \lambda_2 \mu_1 / \lambda_4 \sqrt{\lambda_1}$. \square

Remark 3. Theorem 1 implies that in the absence of measurement noise, the estimation errors uniformly converge to zero as the high-gain parameter decreases, that is, $\lim_{\varepsilon \rightarrow 0} \|\tilde{x}_i\| = 0$. However, owing to the noise of the sensing circuit in a practical MEMS gyroscope, a trade-off between estimation accuracy and noise sensitivity should be taken into account.

4.1 | Stability analysis via LMIs

Assumption 1 is key to obtaining the results of Theorem 1. Therefore, we develop an LMI-based numerical method to construct a Lyapunov function that guarantees this assumption. To this end, regarding the differential equation of the estimation error (16) as a Lurie system, we recast the problem as a standard absolute stability analysis.^{29,30} Instrumental in the development of our method is the modeling of the functions $\phi_i(\cdot)$ as sector-bounded nonlinearities.

Remark 4. The function $\phi_i(\cdot)$ belongs globally to the sector $[0, 1 - \sigma^i]$. That is, for all $z \in \mathbb{R}^3$, we have

$$0 \leq z^\top \phi_i(z) \leq (1 - \sigma^i) z^\top z. \quad (22)$$

The sector condition (22) can be rephrased as the following set of inequalities (see the works of Khalil²⁹ and Boyd et al³⁰):

$$\phi_i^\top(\zeta) \phi_i(\zeta) - (1 - \sigma^i) \eta^\top C_0^\top \phi_i(\zeta) \leq 0, i = 1, 2, 3. \quad (23)$$

We now search for a Lurie-type Lyapunov function of the form

$$V(\eta) = \eta^\top P \eta + 2 \sum_{i=1}^3 \sum_{j=1}^3 \gamma_{ij} \int_0^{\zeta_j} \phi_{ij}(z) dz,$$

with $P \in \mathbb{R}^{9 \times 9}$ being positive definite and $\gamma_{ij} \geq 0$. To guarantee the exponential stability of the origin of Equation 16, for some positive β , we require that

$$\left. \frac{dV(\eta)}{dt} \right|_{(16)} \leq -\frac{\beta}{\varepsilon} \eta^\top \eta. \quad (24)$$

From the stability condition (24), we obtain the following quadratic inequality:

$$\eta^\top (PA_0(\varepsilon) + A_0^\top(\varepsilon)P + \beta I) \eta + 2 \sum_{i=1}^3 \eta^\top (PF_i + A_0(\varepsilon)^\top C_0^\top \Gamma_i) \phi_i(\zeta) + 2 \sum_{i=1}^3 \sum_{j=1}^3 \phi_i^\top(\zeta) \Gamma_i C_0 F_j \phi_j(\zeta) \leq 0, \quad (25)$$

where $\Gamma_i := \text{diag}(\gamma_{ij})_{j=1}^3$, $i = 1, 2, 3$.

Theorem 2. Given $\beta > 0$, assume that there exist a positive-definite matrix $P \in \mathbb{R}^{9 \times 9}$, positive-semidefinite diagonal matrices $\Gamma_i \in \mathbb{R}^{3 \times 3}$, and scalars $\tau_i > 0$ satisfying the LMI

$$\begin{bmatrix} \Lambda_{11} & \Lambda_{12} & \Lambda_{13} & \Lambda_{14} \\ * & \Lambda_{22} & \Lambda_{23} & \Lambda_{24} \\ * & * & \Lambda_{33} & \Lambda_{34} \\ * & * & * & \Lambda_{44} \end{bmatrix} \leq 0, \quad (26)$$

where

$$\begin{aligned} \Lambda_{11} &= PA_0(\varepsilon) + A_0^\top(\varepsilon)P + \beta I, \\ \Lambda_{(i+1)(i+1)} &= \Gamma_i C_0 F_i + F_i^\top C_0^\top \Gamma_i - \tau_i I, i = 1, 2, 3, \\ \Lambda_{1(i+1)} &= PF_i + A_0^\top C_0^\top \Gamma_i + \tau_i \frac{(1 - \sigma^i)}{2} C_0, i = 1, 2, 3, \\ \Lambda_{23} &= \Gamma_1 C_0 F_2 + F_1^\top C_0^\top \Gamma_2, \\ \Lambda_{24} &= \Gamma_1 C_0 F_3 + F_1^\top C_0^\top \Gamma_3, \\ \Lambda_{34} &= \Gamma_2 C_0 F_3 + F_2^\top C_0^\top \Gamma_3. \end{aligned}$$

Then, the system (16) has a globally exponentially stable equilibrium at the origin.

Proof. The nominal error system (16) is exponentially stable at the origin if quadratic inequality (25) holds for all η and ϕ_i satisfying sector condition (23). According to the S-procedure,³⁰ this condition is verified if the following inequality holds for some $\tau_i > 0$:

$$\begin{aligned} &\eta^\top (PA_0(\varepsilon) + A_0^\top(\varepsilon)P + \beta I) \eta + 2 \sum_{i=1}^3 \eta^\top (PF_i + A_0(\varepsilon)^\top C_0^\top \Gamma_i) \phi_i(\zeta) \\ &+ 2 \sum_{i=1}^3 \sum_{j=1}^3 \phi_i^\top(\zeta) \Gamma_i C_0 F_j \phi_j(\zeta) - \sum_{i=1}^3 \tau_i (\phi_i^\top(\zeta) \phi_i(\zeta) - (1 - \sigma^i) \eta^\top C_0^\top \phi_i(\zeta)) \leq 0. \end{aligned} \quad (27)$$

This inequality is rephrased as the feasibility of LMI (26) for a positive-definite matrix P , diagonal positive-semidefinite matrices Γ_i , and nonnegative scalars τ_i . \square

5 | NOMINAL REGULATOR DESIGN

Associated with the equation of motion (8), we define the following composite system as the nominal counterpart of Σ_c :

$$\Sigma_c^n : \begin{cases} \ddot{q} + D_n \dot{q} + K_n q = u_n, \\ \ddot{q}_m + K_m q_m = 0. \end{cases} \quad (28)$$

According to the geometric interpretation given in Section 3, the nominal output regulation of the gyroscope is equivalent to the stabilization of the manifold \mathcal{M} for Σ_c^n . To this end, we need to define an appropriate coordinate to characterize the attractivity of the manifold \mathcal{M} for the trajectories of Σ_c^n . Then, by controlling this coordinate to zero, the output regulation of the gyroscope is carried out. Considering the regulator equation (4), a possible candidate for such a distance coordinate is $q - q_s$. Using the input transformation $u_n - u_s^n$, controlling this distance coordinate to zero corresponds to the well known feedforward design. Owing to the direct dependence of this distance coordinate on the solutions of the regulator

equations, the method is sensitive to perturbations of the nominal gyroscope model (8).¹⁸ This makes the nominal regulator vulnerable to the estimation errors of the disturbance rejection loop. To overcome this issue, we follow a different design paradigm resembling the internal model approach.^{17,18} For this, considering a sufficiently smooth trajectory $q(t)$, we introduce the following transformed variable:

$$q_t(t) := \ddot{q}(t) + K_m q(t). \quad (29)$$

Proposition 1. For Σ_c^n , $q_t(t) = 0$ for all $t \in \mathbb{R}^+$, if and only if $\text{col}(q, \dot{q}, q_m, \dot{q}_m) \in \mathcal{M}$.

Proof. Associated with the reference dynamics (3), we consider the following differential operator:

$$\frac{d^2}{dt^2}(\cdot)I + K_m. \quad (30)$$

The motion of the gyroscope system trajectories on \mathcal{M} , under the control input u_s^n , is equivalent to the immersion of Σ_c^n into the reference dynamics (3). The operator (30) maps any reference trajectory $q_m(\cdot)$ to zero. Thereby, the set of all trajectories $q(\cdot)$ evolving on the manifold \mathcal{M} corresponds to the kernel of the operator (30). On this basis, the variable q_t acts as an indicator function for the set $\{q : \mathbb{R}^+ \rightarrow \mathbb{R}^3 | \ddot{q}(t) + K_m q(t) \equiv 0\}$. That is, a vibration trajectory $q(\cdot)$ evolves on \mathcal{M} if and only if its transformation $q_t(\cdot)$ is equivalent to zero. \square

According to Proposition 1, q_t is conceived as a dynamic measure of distance between the trajectories of Σ_c^n and the target manifold \mathcal{M} . By replicating an internal model of the reference dynamics, this distance coordinate does not explicitly depend on the solutions of regulator equations and, therefore, enables a robust design. To obtain the dynamics of q_t , we apply the operator (30) to the nominal system (8):

$$\ddot{q}_t + D_n \dot{q}_t + K_n q_t = u_t, \quad (31)$$

where the following control transformation is used:

$$u_t := \ddot{u}_n + K_m u_n. \quad (32)$$

Since q_t depends on the acceleration vector, we cannot use it for feedback purposes. To associate q_t with the tracking error, we apply the operator (30) to the tracking error (5):

$$\ddot{e} + K_m e = q_t. \quad (33)$$

Using the augmented state vector $x_a := \text{col}(q_t, \dot{q}_t, e, \dot{e}) \in \mathbb{R}^{12}$, both Equations 31 and 33 are lumped to the following state equation:

$$\begin{aligned} \dot{x}_a &= A_a x_a + B_a u_t, \\ e &= C_a x_a, \end{aligned} \quad (34)$$

where

$$A_a = \begin{bmatrix} O & I & O & O \\ -K_n & -D_n & O & O \\ O & O & O & I \\ I & O & -K_m & O \end{bmatrix}, B_a = \begin{bmatrix} O \\ I \\ O \\ O \end{bmatrix}, C_a = [O \quad O \quad I \quad O].$$

Proposition 2. System (34) is both controllable and observable.

Proof. For all $s \in \mathbb{C}$, $\text{rank}[sI - A_a \ B_a] = 12$ and $\text{rank}[sI - A_a^\top \ C_a^\top] = 12$. By the Popov-Belevitch-Hauth rank test, the system is both controllable and observable. \square

To stabilize the augmented system (34), we use the observer-based output feedback controller

$$\begin{aligned} \dot{\hat{x}}_a &= A_a \hat{x}_a + B_a u_t + L(e - C_a \hat{x}_a), \\ u_t &= -G \hat{x}_a, \end{aligned} \quad (35)$$

where $\hat{x}_a \in \mathbb{R}^{12}$ is the estimate of x_a , and G and L are design matrices of suitable dimensions. Setting $x_s := \text{col}(x_a, \hat{x}_a)$, we obtain a closed-loop system governed by the following equation:

$$\dot{x}_s = A_s x_s, \quad (36)$$

where

$$A_s = \begin{bmatrix} A_a & -B_a G \\ LC_a & A_a - B_a G - LC_a \end{bmatrix}.$$

By Proposition 2, there always exist gain matrices G and L that render the system (36) exponentially stable. Therefore, we make the following assumption.

Assumption 2. The controller (35) is designed such that all eigenvalues of matrix A_s are in the open left-half complex plane.

Remark 5. The proposed control method uses the auxiliary control variable u_t to regulate the gyroscope output. The primary control input u_n is obtained by applying the inverse of the operator (30) to u_t . This amounts to solving the differential equation (32) for u_n while u_t is obtained from the controller (35).

5.1 | Robust stabilization

In this section, we study the effect of the disturbance rejection loop on controlling the distance coordinate q_t to zero. Considering the control law (9) with the disturbance estimate $\hat{\Delta}(t) = \hat{x}_3(t)$, the equation of motion of the nominal system (8) becomes

$$\ddot{q} + D_n \dot{q} + K_n q = u_n + \tilde{x}_3(t). \quad (37)$$

By defining the signal $\xi_t(t) := d^2 \tilde{x}_3(t)/dt^2 + K_m \tilde{x}_3(t)$ and taking the measurement noise into account, we rewrite the closed-loop equation (36) in the following perturbed form:

$$\dot{x}_s = A_s x_s + B_\xi \xi_t(t) + B_\theta \theta(t), \quad (38)$$

where

$$B_\xi = \begin{bmatrix} B_a \\ O \end{bmatrix}, \quad B_\theta = \begin{bmatrix} O \\ L \end{bmatrix}.$$

Compared with the feedforward design, the disturbance estimation error affects the proposed regulation method via the transformed signal $\xi_t(\cdot)$ rather than $\tilde{x}_3(\cdot)$. By the incorporated internal model property, operator (30) annihilates the components of $\tilde{x}_3(\cdot)$ with the same frequency content as the reference signal. As a result, the structural robustness of the closed-loop system is improved. To further suppress the effect of the disturbance estimation error, we use the energy-to-peak robust control.^{31,32} By this method, the peak (\mathcal{L}_∞ -norm) of the desired performance variable can be restricted to a specific level, considering the energy (\mathcal{L}_2 -norm) of the disturbance. On this basis, to obtain an appropriate transient response and a robust performance, controller (35) is designed under the following specifications.

1. Given $0 < a < b$, all eigenvalues of the matrix A_s are confined to the following region in the complex plane:

$$\mathcal{D}_s = \{s \in \mathbb{C} \mid -b \leq \Re(s) \leq -a\}. \quad (39)$$

2. To attenuate the effect of the perturbations on the tracking error, assuming \mathcal{L}_2 -bounded signals $\xi_t(\cdot)$ and $\theta(\cdot)$, the following energy-to-peak performance criterion is required to hold for the given indices $v_1 > 0$ and $v_2 > 0$:

$$\|e(\cdot)\|_{\mathcal{L}_\infty} < v_1 \|\xi_t(\cdot)\|_{\mathcal{L}_2} + v_2 \|\theta(\cdot)\|_{\mathcal{L}_2}. \quad (40)$$

Lemma 1. (Skelton et al³¹ and Zhang et al³²)

The following linear system is considered:

$$\begin{aligned}\dot{\bar{x}} &= \bar{A}\bar{x} + \bar{B}\varpi, \\ \bar{z} &= \bar{C}\bar{x},\end{aligned}\quad (41)$$

where \bar{x} is the state vector, ϖ is the external input, and \bar{z} is the performance output. Assuming that the \mathcal{L}_2 -norm of ϖ is bounded, the energy-to-peak norm inequality $\|\bar{z}(\cdot)\|_{\mathcal{L}_\infty} < \bar{v}\|\varpi(\cdot)\|_{\mathcal{L}_2}$ is verified if and only if there exists a positive-definite matrix \bar{P} satisfying

$$\begin{bmatrix} \bar{P}\bar{A} + \bar{A}^\top \bar{P} & \bar{P}\bar{B} \\ \bar{B}^\top \bar{P} & -I \end{bmatrix} < 0, \quad (42a)$$

$$\begin{bmatrix} -\bar{v}^2 I & \bar{C} \\ \bar{C}^\top & -\bar{P} \end{bmatrix} < 0. \quad (42b)$$

Proof. By Theorem 4.6.2 of Skelton et al,³¹ the energy-to-peak performance $\|\bar{z}(\cdot)\|_{\mathcal{L}_\infty} < \bar{v}\|\varpi(\cdot)\|_{\mathcal{L}_2}$ holds if and only if the following inequalities are satisfied for a positive-definite matrix \bar{R} :

$$\bar{A}\bar{R} + \bar{R}\bar{A}^\top + \bar{B}\bar{B}^\top < 0, \quad (43a)$$

$$\bar{C}\bar{R}\bar{C}^\top < \bar{v}^2 I. \quad (43b)$$

Applying a congruence transformation to Equation 43a with \bar{R}^{-1} and using the Schur complement, we obtain

$$\begin{bmatrix} \bar{R}^{-1}\bar{A} + \bar{A}^\top \bar{R}^{-1} & \bar{R}^{-1}\bar{B} \\ \bar{B}^\top \bar{R}^{-1} & -I \end{bmatrix} < 0. \quad (44)$$

Furthermore, the inequality (43b) is equivalent to

$$\begin{bmatrix} -\bar{v}^2 I & \bar{C} \\ \bar{C}^\top & -\bar{R}^{-1} \end{bmatrix} < 0. \quad (45)$$

Setting $\bar{P} = \bar{R}^{-1}$, we obtain the inequalities (43a) and (43b) from Equations 44 and 45, respectively. \square

Lemma 2. (Young's inequality)

For matrices X and Y with compatible dimensions, the inequality

$$X^\top Y + Y^\top X \leq \epsilon X^\top \bar{Q} X + \frac{1}{\epsilon} Y^\top \bar{Q}^{-1} Y \quad (46)$$

holds for any positive-definite matrix \bar{Q} and any number $\epsilon > 0$.

Proof. For any matrices \bar{Q}_1 and \bar{Q}_2 of appropriate dimensions, we have

$$\left(\sqrt{\epsilon} \bar{Q}_1 X - \frac{1}{\sqrt{\epsilon}} \bar{Q}_2 Y \right)^\top \left(\sqrt{\epsilon} \bar{Q}_1 X - \frac{1}{\sqrt{\epsilon}} \bar{Q}_2 Y \right) \geq 0,$$

which gives

$$X^\top \bar{Q}_1^\top \bar{Q}_2 Y + Y^\top \bar{Q}_2^\top \bar{Q}_1 X \leq \epsilon X^\top \bar{Q}_1^\top \bar{Q}_1 X + \frac{1}{\epsilon} Y^\top \bar{Q}_2^\top \bar{Q}_2 Y. \quad (47)$$

Imposing the condition $\bar{Q}_1^\top \bar{Q}_2 = I$ yields $(\bar{Q}_2^\top \bar{Q}_2)(\bar{Q}_1^\top \bar{Q}_1) = \bar{Q}_1^\top \bar{Q}_2 = I$ and $\bar{Q}_2^\top \bar{Q}_2 = (\bar{Q}_1^\top \bar{Q}_1)^{-1}$. Therefore, the inequality (46) is obtained from (47) by setting $\bar{Q} = \bar{Q}_1^\top \bar{Q}_1$. \square

Lemma 3. Consider the linear system (41). All eigenvalues of \bar{A} belong to \mathcal{D}_s if and only if there exists a positive-definite matrix \bar{P} satisfying

$$\bar{P}\bar{A} + \bar{A}^\top \bar{P} + 2a\bar{P} \leq 0, \quad (48a)$$

$$\bar{P}\bar{A} + \bar{A}^\top \bar{P} + 2b\bar{P} \geq 0. \quad (48b)$$

Proof. We note that $\text{eig}(\bar{A}) \subset \mathcal{D}_s$ if and only if $\Re(s_1) \leq 0$ and $\Re(s_2) \geq 0$ for all $s_1 \in \text{eig}(\bar{A} + aI)$ and $s_2 \in \text{eig}(\bar{A} + bI)$. By Lyapunov's theorem on the stability of linear system,^{28,29} this condition is equivalent to the existence of a positive definite matrix \bar{P} satisfying the LMIs (48a) and (48b). \square

Theorem 3. Given $v_1 > 0$, $v_2 > 0$, and $\epsilon > 0$, assume that there exist positive-definite matrices R_1 and P_2 and matrices W_1 and W_2 that satisfy the following LMIs:

$$\begin{bmatrix} \mathcal{Z}_1 & \mathcal{Z}_2 \\ \mathcal{Z}_2^\top & -\mathcal{Z}_3 \end{bmatrix} < 0, \quad (49a)$$

$$\begin{bmatrix} -v_1^2 I & C_a R_1 & O \\ R_1 C_a^\top & -R_1 & O \\ O & O & -P_2 \end{bmatrix} < 0, \quad (49b)$$

$$A_a R_1 + R_1 A_a^\top - B_a W_1 - W_1^\top B_a^\top + 2a R_1 \leq 0, \quad (49c)$$

$$A_a R_1 + R_1 A_a^\top - B_a W_1 - W_1^\top B_a^\top + 2b R_1 \geq 0, \quad (49d)$$

$$P_2 A_a + A_a^\top P_2 - W_2 C_a - C_a^\top W_2^\top + 2a P_2 \leq 0, \quad (49e)$$

$$P_2 A_a + A_a^\top P_2 - W_2 C_a - C_a^\top W_2^\top + 2b P_2 \geq 0, \quad (49f)$$

where

$$\begin{aligned} \mathcal{Z}_1 &:= \begin{bmatrix} A_a R_1 + R_1 A_a^\top - B_a W_1 - W_1^\top B_a^\top & * & * & * \\ O & P_2 A_a + A_a^\top P_2 - W_2 C_a - C_a^\top W_2^\top & * & * \\ B_a^\top & B_a^\top P_2 & -I & * \\ O & -\frac{v_1}{v_2} W_2^\top & O & -I \end{bmatrix}, \\ \mathcal{Z}_2 &:= \text{diag}(B_a W_1, I, O, O), \\ \mathcal{Z}_3 &:= \text{diag}\left(\frac{1}{\epsilon} R_1, \epsilon R_1, I, I\right). \end{aligned}$$

Then, the observer-based controller (35) with $G = W_1 R_1^{-1}$ and $L = P_2^{-1} W_2$ ensures that the energy-to-peak performance criterion (40) is satisfied and all eigenvalues of matrix A_s are confined to the region \mathcal{D}_s .

Proof. Here, we introduce the following arguments.

1. First, we note that the energy-to-peak performance inequality (40) holds if $\|e(\cdot)\|_{\mathcal{L}_\infty} < v_1 \|\omega_s(\cdot)\|_{\mathcal{L}_2}$ for $\omega_s(\cdot) := \text{col}(\xi_t(\cdot), v_2/v_1 \vartheta(\cdot))$. On this basis, using the estimation error $\tilde{x}_a := x_a - \hat{x}_a$, we rewrite the perturbed dynamics (38) in the following form:

$$\begin{bmatrix} \dot{\tilde{x}}_a \\ \dot{\hat{x}}_a \end{bmatrix} = \begin{bmatrix} A_a - B_a G & B_a G \\ O & A_a - LC_a \end{bmatrix} \begin{bmatrix} \tilde{x}_a \\ \hat{x}_a \end{bmatrix} + \begin{bmatrix} B_a & O \\ B_a & -\frac{v_1}{v_2} L \end{bmatrix} \omega_s(t). \quad (50)$$

Applying Lemma 1 with $\bar{P} = \text{diag}(P_1, P_2)$ to system (50), we obtain the following bilinear matrix inequality from Equation 42a:

$$\begin{bmatrix} P_1(A_a - B_a G) + (A_a - B_a G)^\top P_1 & * & * & * \\ (P_1 B_a G)^\top & P_2(A_a - LC_a) + (A_a - LC_a)^\top P_2 & * & * \\ (P_1 B_a)^\top & (P_2 B_a)^\top P_2 & -I & * \\ O & -\frac{v_1}{v_2} (P_2 L)^\top & O & -I \end{bmatrix} < 0. \quad (51)$$

The main obstacle to linearize the inequality (51) is the presence of the coupling term $P_1 B_a G$.³³ To solve this problem, defining $R_1 = P_1^{-1}$ and applying a congruence transformation with $\text{diag}(R_1, I, I, I)$ to Equation 51, we have

$$\mathcal{Z}_1 + \begin{bmatrix} B_a G \\ O \\ O \\ O \end{bmatrix} \begin{bmatrix} O \\ I \\ O \\ O \end{bmatrix}^\top + \begin{bmatrix} O \\ I \\ O \\ O \end{bmatrix} \begin{bmatrix} B_a G \\ I \\ O \\ O \end{bmatrix}^\top < 0. \quad (52)$$

Using Lemma 2, we get the following inequality:

$$\begin{bmatrix} B_a G \\ O \\ O \\ O \end{bmatrix} \begin{bmatrix} O \\ I \\ O \\ O \end{bmatrix}^\top + \begin{bmatrix} O \\ I \\ O \\ O \end{bmatrix} \begin{bmatrix} B_a G \\ I \\ O \\ O \end{bmatrix}^\top \leq \epsilon \begin{bmatrix} B_a G \\ O \\ O \\ O \end{bmatrix} R_1 \begin{bmatrix} B_a G \\ O \\ O \\ O \end{bmatrix}^\top + \frac{1}{\epsilon} \begin{bmatrix} O \\ I \\ O \\ O \end{bmatrix} R_1^{-1} \begin{bmatrix} O \\ I \\ O \\ O \end{bmatrix}^\top, \quad (53)$$

with ϵ being a positive constant. With the change of variables $W_1 = GR_1$ and $W_2 = P_2 L$, the right-hand side of the inequality (53) is equivalent to $Z_2 Z_3^{-1} Z_2^\top$. Accordingly, the inequality (51) holds if $Z_2 + Z_2 Z_3^{-1} Z_2^\top < 0$. By the Schur complement analysis, we obtain LMI (49a).

2. Inequality (42b) of Lemma 1 for system (50) yields

$$\begin{bmatrix} -v_1^2 I & C_a & O \\ C_a^\top & -P_1 & O \\ O & O & -P_2 \end{bmatrix} < 0.$$

Applying a congruence transformation with $\text{diag}(I, R_1, I)$, we obtain LMI (49b).

3. Owing to the separation principle, $\text{eig}(A_s) = \text{eig}(A_a - B_a G) \cup \text{eig}(A_a - LC_a)$. Therefore, $\text{eig}(A_s) \subset \mathcal{D}_s$ if and only if $\text{eig}(A_a - B_a G) \subset \mathcal{D}_s$ and $\text{eig}(A_a - LC_a) \subset \mathcal{D}_s$. In this regard, applying Lemma 3 with $\bar{P} = P_1$ to $A_a - B_a G$, we have

$$P_1(A_a - B_a G) + (A_a - B_a G)^\top P_1 + 2aP_1 \leq 0, \quad (54a)$$

$$P_1(A_a - B_a G) + (A_a - B_a G)^\top P_1 + 2bP_1 \geq 0. \quad (54b)$$

Performing a congruence transformation with R_1 , we get LMIs (49c) and (49d). Similarly, the application of Lemma 3 with $\bar{P} = P_2$ to $A_a - LC_a$ yields LMIs (49e) and (49f). \square

6 | CLOSED-LOOP STABILITY

The overall block diagram of the proposed control system is shown in Figure 2. The modular structure of the control system allows a separate design and analysis of the nominal output regulation and the disturbance rejection loops. However, the interaction of these components in the closed-loop operation still needs to be examined. The results of Theorems 1 and 2 establish the convergence and stability of the ESO-based disturbance rejection loop. Accordingly, we consider the effect of disturbance rejection-based control law (9), with $\hat{\Delta}(\cdot) = \hat{x}_3(\cdot)$, on the performance of the nominal closed-loop system. The nominal closed-loop system, operating in conjunction with the disturbance rejection loop, is governed by the following differential equations:

$$\begin{aligned} \dot{x}_m &= A_m x_m, \\ \dot{x}_{cl} &= A_{cl} x_{cl} + B_1 x_m + B_2 \tilde{x}_3(t) + B_3 \vartheta(t), \end{aligned} \quad (55)$$

where $x_m := \text{col}(q_m, \dot{q}_m)$, $x_{cl} := \text{col}(q, \dot{q}, u_n, \hat{u}_n, \hat{x}_a)$ and

$$\begin{aligned} A_m &= \begin{bmatrix} O & I \\ -K_m & O \end{bmatrix}, \quad A_{cl} = \begin{bmatrix} O & I & O & O & O \\ -K_n & -D_n & I & O & O \\ O & O & O & I & O \\ O & O & -K_m & O & -G \\ L & O & O & O & A_a - B_a G - LC_a \end{bmatrix}, \quad B_1 = \begin{bmatrix} O \\ O \\ O \\ O \\ -LC_m \end{bmatrix}, \\ B_2 &= \begin{bmatrix} O \\ I \\ O \\ O \\ O \end{bmatrix}, \quad B_3 = \begin{bmatrix} O \\ O \\ O \\ O \\ L \end{bmatrix}. \end{aligned}$$

To proceed with the closed-loop stability analysis, we introduce the following lemma.

Lemma 4. *Matrices A_s and A_{cl} are similar.*

Proof. Matrix A_{cl} has the following block structure:

$$A_{cl} = \begin{bmatrix} A' & -B'G \\ LC' & A_a - B_a G - LC_a \end{bmatrix},$$

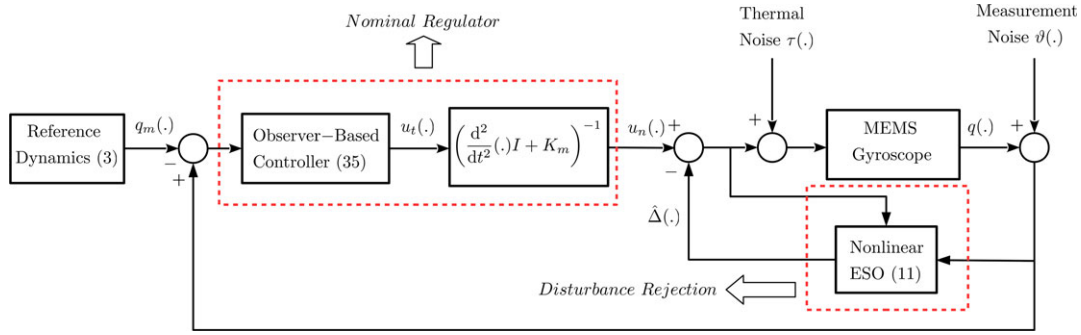


FIGURE 2 Block diagram of the closed-loop system. (ESO: extended state observer; MEMS: microelectromechanical system) [Colour figure can be viewed at wileyonlinelibrary.com]

where

$$A' = \begin{bmatrix} O & I & O & O \\ -K_n & -D_n & I & O \\ O & O & O & I \\ O & O & -K_m & O \end{bmatrix}, \quad B' = \begin{bmatrix} O \\ O \\ O \\ I \end{bmatrix}, \quad C' = [I \ O \ O \ O].$$

Since A_a and A' are block lower and block upper triangular matrices, respectively, with the same diagonal blocks, we have $\text{eig}(A_a) = \text{eig}(A')$. Moreover, for all $s \in \mathbb{C}$, we have

$$C'(sI - A')^{-1}B' = C_a(sI - A_a)^{-1}B_a.$$

Thereby, (A', B', C') and (A_a, B_a, C_a) can be conceived as 2 different realizations of the same transfer matrix. Accordingly, there is a nonsingular matrix T' such that $A' = T'A_aT'^{-1}$, $B' = T'B_a$, and $C' = C_aT'^{-1}$. Using $T := \text{diag}(T', I)$, we obtain the similarity transformation $A_{cl} = TA_sT^{-1}$. \square

Theorem 4. Assume that Assumptions 1 and 2 are satisfied; let $\lambda_0 := -\max_{s \in \text{eig}(A_{cl})} \Re(s)$ and $\lambda'_0 := \lambda_4/2\lambda_2$ be a constant associated with the ESO convergence rate as given in the inequality (21). Then, the following statements hold:

1. The state trajectory $x_{cl}(\cdot)$ is bounded.
2. In the state space of Σ_c , the gyroscope state $\text{col}(q(\cdot), \dot{q}(\cdot))$ converges practically to the manifold \mathcal{M} . More specifically

$$\|\text{col}(q(t), \dot{q}(t)) - \text{col}(q_s(t), \dot{q}_s(t))\| \leq \bar{\mu}_0 \exp(-\lambda_0 t) + \bar{\mu}_1 \exp\left(-\frac{\lambda'_0 t}{\varepsilon}\right) + \bar{\mu}_2 \frac{\vartheta_0}{\varepsilon^2} + \varepsilon \bar{\mu}_3 h_0, \quad (56)$$

for all $t \in \mathbb{R}^+$ and for some positive constants $\bar{\mu}_0$, $\bar{\mu}_1$, $\bar{\mu}_2$, and $\bar{\mu}_3$.

3. The control input (9) converges practically to the steady-state value u_s in the following sense:

$$\|u(t) - u_s(t)\| \leq \bar{\mu}'_0 \exp(-\lambda_0 t) + \bar{\mu}'_1 \exp\left(-\frac{\lambda'_0 t}{\varepsilon}\right) + \bar{\mu}'_2 \frac{\vartheta_0}{\varepsilon^2} + \varepsilon \bar{\mu}'_3 h_0, \quad (57)$$

for all $t \in \mathbb{R}^+$ and some positives $\bar{\mu}'_0$, $\bar{\mu}'_1$, $\bar{\mu}'_2$, and $\bar{\mu}'_3$.

Proof. Here, we introduce the following arguments.

1. The following unperturbed closed-loop dynamics is considered:

$$\dot{x}_m = A_m x_m, \quad (58a)$$

$$\dot{x}_{cl} = A_{cl} x_{cl} + B_1 x_m. \quad (58b)$$

In view of Lemma 4 and Assumption 2, all eigenvalues of matrix A_{cl} are in the open left-half of the complex plane, whereas all eigenvalues of A_m lie on the imaginary axis. According to the center manifold theorem,^{18,28} in the extended state space of the systems (58a) and (58b), there is a stable invariant manifold \mathcal{M}_{cl} that attracts all the trajectories of Equation 58b with an exponential convergence rate. The motion of the trajectories on \mathcal{M}_{cl} corresponds to the immersion of the system (58b) into (58a). As a result, there exists a linear map $x_{cl} = \Pi x_m$ satisfying the immersion condition, as follows:

$$\Pi A_m = A_{cl} \Pi + B_1. \quad (59)$$

This condition is a Sylvester matrix equation, and since $\text{eig}(A_m) \cap \text{eig}(A_{cl}) = \emptyset$, the existence of a unique solution Π is guaranteed.¹⁷ Accordingly, we consider $z_{cl} := x_{cl} - \Pi x_m$ as a distance function with respect to \mathcal{M}_{cl} . Now, referring to the perturbed closed-loop dynamics (55), we obtain

$$\dot{z}_{cl} = A_{cl}z_{cl} + B_2\tilde{x}_3(t) + B_3\vartheta(t). \quad (60)$$

Thereby

$$z_{cl}(t) = \exp(A_{cl}t)z_{cl}(0) + \int_0^t \exp(A_{cl}(t-t'))(B_2\tilde{x}_3(t') + B_3\vartheta(t')) dt'.$$

Using the disturbance estimation error bound (21), it follows that the solution of the system (60), for all $t \in \mathbb{R}^+$, satisfies an inequality of the form

$$\|z_{cl}(t)\| \leq \bar{\mu}_0 \exp(-\lambda_0 t) + \bar{\mu}_1 \exp\left(-\frac{\lambda'_0 t}{\varepsilon}\right) + \bar{\mu}_2 \frac{\vartheta_0}{\varepsilon^2} + \varepsilon \bar{\mu}_3 h_0, \quad (61)$$

with $\bar{\mu}_0$, $\bar{\mu}_1$, $\bar{\mu}_2$, and $\bar{\mu}_3$ being pertinent positive numbers. Inequality (61) indicates the practical convergence of the closed-loop trajectories to the manifold \mathcal{M}_{cl} . The boundedness of the state trajectory $x_{cl}(\cdot)$ follows from the triangle inequality $\|x_{cl}(t)\| \leq \|z_{cl}(t)\| + \|\Pi x_m(t)\|$.

2. By partitioning the matrix Π according to the components of x_{cl} and x_m , we have

$$\begin{aligned} q &= \Pi_{11}q_m + \Pi_{12}\dot{q}_m, \\ \dot{q} &= \Pi_{21}q_m + \Pi_{22}\dot{q}_m, \\ u_n &= \Pi_{31}q_m + \Pi_{32}\dot{q}_m, \end{aligned} \quad (62)$$

for all $(q, \dot{q}, q_m, \dot{q}_m) \in \mathcal{M}_{cl}$. Comparing Equation 62 with the regulator equations (4), we obtain

$$\Pi_{11} = \Pi_{22} = I, \Pi_{12} = \Pi_{21} = 0, \Pi_{31} = K_n - K_m, \Pi_{32} = D_n.$$

Thereby, we infer that \mathcal{M} is a submanifold of \mathcal{M}_{cl} , and hence, inequality (61) implies the practical convergence of the gyroscope state variables to \mathcal{M} .

3. Owing to Equation 62, the control variable u_n is equivalent to u_n^s as the system trajectories evolve on \mathcal{M}_{cl} . Considering the bounds given by the inequalities (21) and (61), we use the triangle inequality

$$\|u(t) - u_s(t)\| \leq \|u_n(t) - u_n^s(t)\| + \|\tilde{x}_3(t)\|$$

to obtain Equation 57. □

On the basis of Theorems 3 and 4, we state the following corollary regarding the tracking performance of the control system.

Corollary 1. *Suppose Assumptions 1 and 2 are satisfied; the LMIs (49a)-(49f) are feasible, and the observer-based controller (35) is designed according to Theorem 3. Then, the following statements hold:*

1. *The tracking error $e(\cdot)$ and its time derivative $\dot{e}(\cdot)$ are globally bounded and globally ultimately bounded. That is, after a finite transient time t'_0 , we have*

$$\|e^{(i)}(t)\| \leq \rho'_0 + \bar{\mu}_2 \frac{\vartheta_0}{\varepsilon^2} + \varepsilon \bar{\mu}_3 h_0, \quad i = 0, 1, \quad (63)$$

with $\rho'_0 > 0$ being arbitrarily small.

2. *For \mathcal{L}_2 components of the signals $\xi_t(\cdot)$ and $\vartheta(\cdot)$, the tracking error satisfies the energy-to-peak inequality (40).*

Proof. The first part is deduced from inequality (56). The second part follows directly from Theorem 3. □

According to Corollary 1, the ultimate bounds of $e(\cdot)$ and $\dot{e}(\cdot)$ depend on the constants εh_0 and $\vartheta_0/\varepsilon^2$. On the one hand, decreasing the ESO parameter ε attenuates the effect of the total disturbance; on the other hand, it amplifies the contribution of the measurement noise. Therefore, according to Remark 3, a trade-off between steady-state error and sensitivity to measurement noise should be considered in selecting ε .

TABLE 1 Parameters of the simulated microelectromechanical system gyroscope

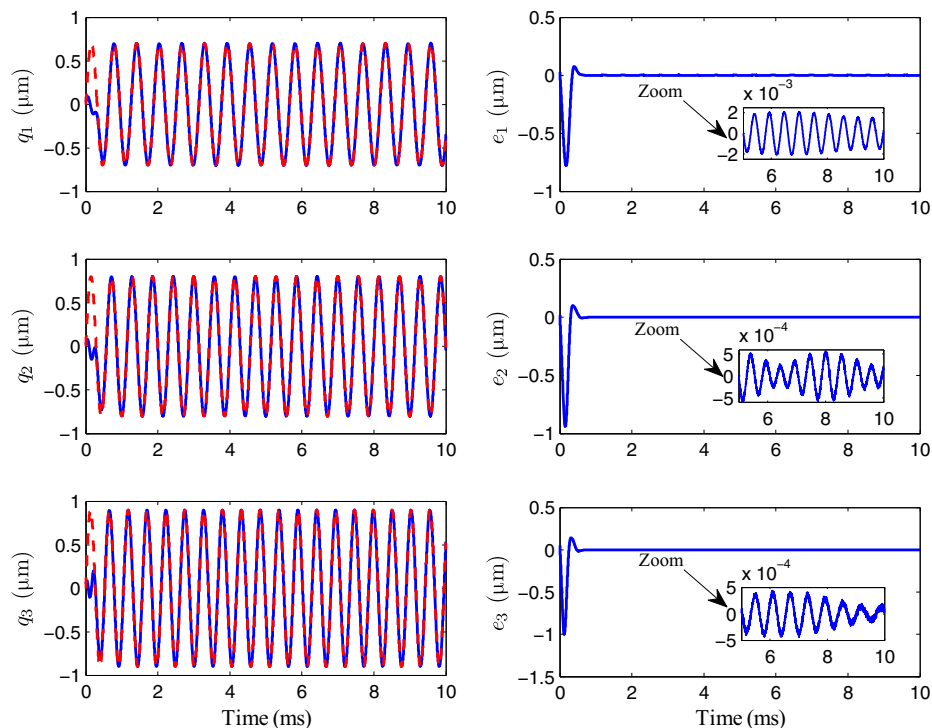
Parameter	Value	Unit	Parameter	Value	Unit
m	5.095×10^{-7}	kg	d_{11}	1.3349×10^{-6}	Ns/m
k_{11}	349.7647	N/m	d_{22}	1.6359×10^{-6}	Ns/m
k_{22}	525.2254	N/m	d_{33}	1.9528×10^{-6}	Ns/m
k_{33}	748.4514	N/m	d_{12}	6.6747×10^{-8}	Ns/m
k_{12}	17.4882	N/m	d_{13}	9.7639×10^{-8}	Ns/m
k_{13}	37.4226	N/m	d_{23}	8.1793×10^{-8}	Ns/m
k_{23}	26.2613	N/m	q_0	10^{-6}	m
α_1	1.5739×10^6	N/m ³	w_0	10^3	Hz
α_2	2.3635×10^6	N/m ³			
α_3	3.3680×10^6	N/m ³			

7 | SIMULATION STUDY

To evaluate the performance of the proposed control method, we conduct numerical simulations using the MATLAB/Simulink environment. The parameters of the simulated MEMS gyroscope are shown in Table 1; the key values are taken from the Massachusetts Institute of Technology-Silicon on Insulator (MIT-SOI) gyroscope data.⁶ Throughout simulations, the off-diagonal stiffness and damping parameters are assumed to be unknown, and the diagonal parameters are allowed to vary by 5% with respect to the nominal values. The input angular velocity is

$$\omega(t) = \begin{bmatrix} 1 + 2 \sin(0.1 w_0 \pi t) + 3 \cos(0.12 w_0 \pi t) \\ 5 \sin(0.2 w_0 \pi t) + 3 \cos(0.13 w_0 \pi t) \\ 3 + 2 \sin(0.15 w_0 \pi t) + 4 \cos(0.3 w_0 \pi t) \end{bmatrix} \left(\frac{\text{rad}}{\text{s}} \right).$$

The thermal noise and measurement noise are considered zero-mean Gaussian white noise signals with power spectral densities of $1.47 \times 10^{-26} \text{ N}^2\text{s}$ and $1.49 \times 10^{-27} \text{ m}^2\text{s}$, respectively.⁶ The off-track generalized coordinates and velocities are assumed to be $q(0) = [3, 2, 5]^\top \times 10^{-8} \text{ (m)}$ and $\dot{q}(0) = [0, 0, 0]^\top \text{ (m/s)}$, respectively. The reference dynamics (3) is

**FIGURE 3** Tracking behavior of the controlled gyroscope axes [Colour figure can be viewed at wileyonlinelibrary.com]

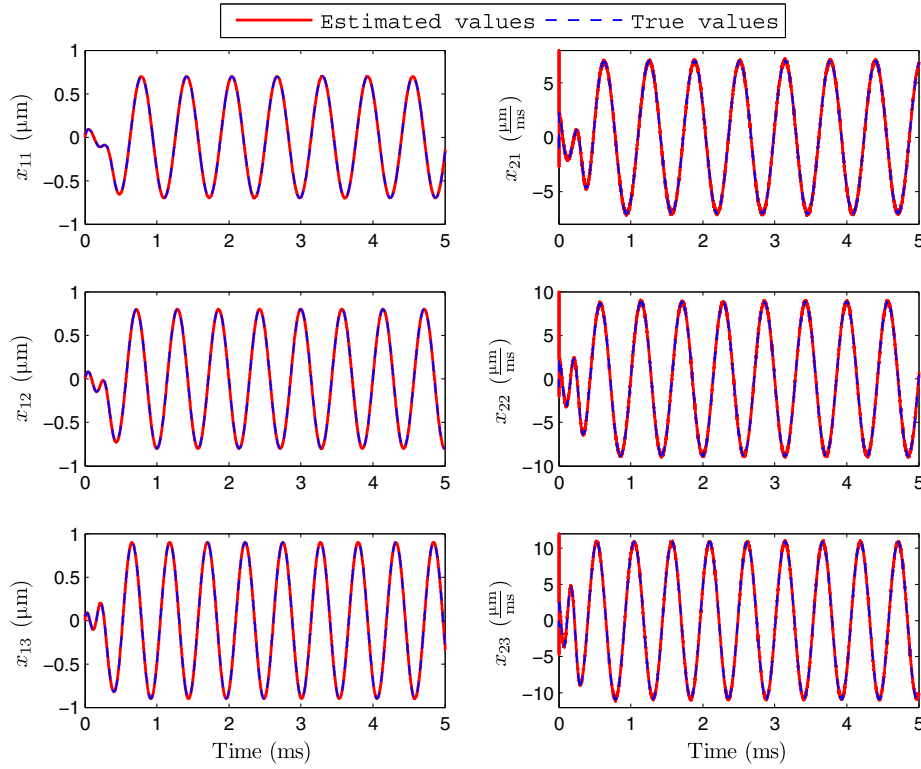


FIGURE 4 Estimation of the generalized coordinates and velocities by the extended state observer equation (11) [Colour figure can be viewed at wileyonlinelibrary.com]

characterized by $K_m = \text{diag}(w_1^2, w_2^2, w_3^2)$, $q_m(0) = [0, 0, 0]^T$, and $\dot{q}_m(0) = [q_1^0 w_1, q_2^0 w_2, q_3^0 w_3]^T$ with the numerical values $w_1 = 10^4 \text{ rad/s}$, $w_2 = 1.1 \times 10^4 \text{ rad/s}$, $w_3 = 1.2 \times 10^4 \text{ rad/s}$, $q_1^0 = 0.7 \text{ } \mu\text{m}$, $q_2^0 = 0.8 \text{ } \mu\text{m}$, and $q_3^0 = 0.9 \text{ } \mu\text{m}$. The high-gain parameter of observer (11) is selected as $\epsilon = 2 \times 10^{-4}$. The nonlinear gain functions, defined by (15), are designed with the parameters $\sigma = 0.65$ and $d = 0.01$. The matrices H_i are designed such that the eigenvalues of the Jacobian matrix of the error dynamics (16), $A_0(\epsilon) + \sum_{i=1}^3 (1 - \sigma^i) F_i C_0$, are placed on $\{-1 - i/2\}_{i=0}^8$. To prevent the system from peaking, the estimated disturbances are saturated as $\hat{\Delta}_i \leq 5.095 \times 10^{-4} \text{ N}$.²⁷ In view of Theorem 2, to establish the convergence results of Theorem 1, the solvability of the LMI (26) is investigated for the specified observer parameters with the convergence rate of $\beta = 0.3$. For this purpose, we use CVX, which is a MATLAB package for solving convex programming problems.^{34,35} Thus

$$\begin{aligned} \lambda_{\min}(P) &= 0.3023, \quad \lambda_{\max}(P) = 161.4710, \quad \Gamma_1 = \text{diag}(169.9819, 192.5589, 197.3694), \\ \Gamma_2 &= \text{diag}(133.3404, 121.7049, 105.1653), \quad \Gamma_3 = \text{diag}(5.4353, 8.4049, 5.8404), \\ \tau_1 &= 6.4378 \times 10^3, \quad \tau_2 = 8.5993 \times 10^3, \quad \tau_3 = 5.6626 \times 10^3. \end{aligned}$$

The results guarantee the exponential stability of the origin of the system (16). The observer-based output feedback controller (11) is designed according to Theorem 3 by taking the parameters $\epsilon = 10^{-2}$, $v_1 = 10^{-1}$, and $v_1/v_2 = 10^{-3}$ and the desired region $\mathcal{D}_s = \{s \in \mathbb{C} | -20 \leq \Re(s) \leq -7\}$ for the closed-loop eigenvalues. With these parameters, the LMIs (49a)–(49f) are solved using CVX. To illustrate the tracking performance of the control system, Figure 3 shows the controlled trajectory of the proof mass alongside the corresponding tracking errors. It is observed that after a transient time of 1 ms, the gyroscope vibration follows the reference motion with small errors. To evaluate the performance of the designed ESO (11), Figure 4 shows the time trajectories of the estimated position and velocity signals. Moreover, to highlight the noise robustness of the nonlinear ESO, its estimation error is compared with the conventional linear ESO (that is, $g_i(z) = z$) by Figure 5. The results show that the proposed nonlinear gain functions improve the attenuation of the measurement noise, with respect to the linear differentiators, especially in the case of velocity and disturbance estimation. The overall control inputs applied to the proof mass are shown in Figure 6. The performance of the control method is compared to the conventional linear ADRC.⁷ The linear ADRC

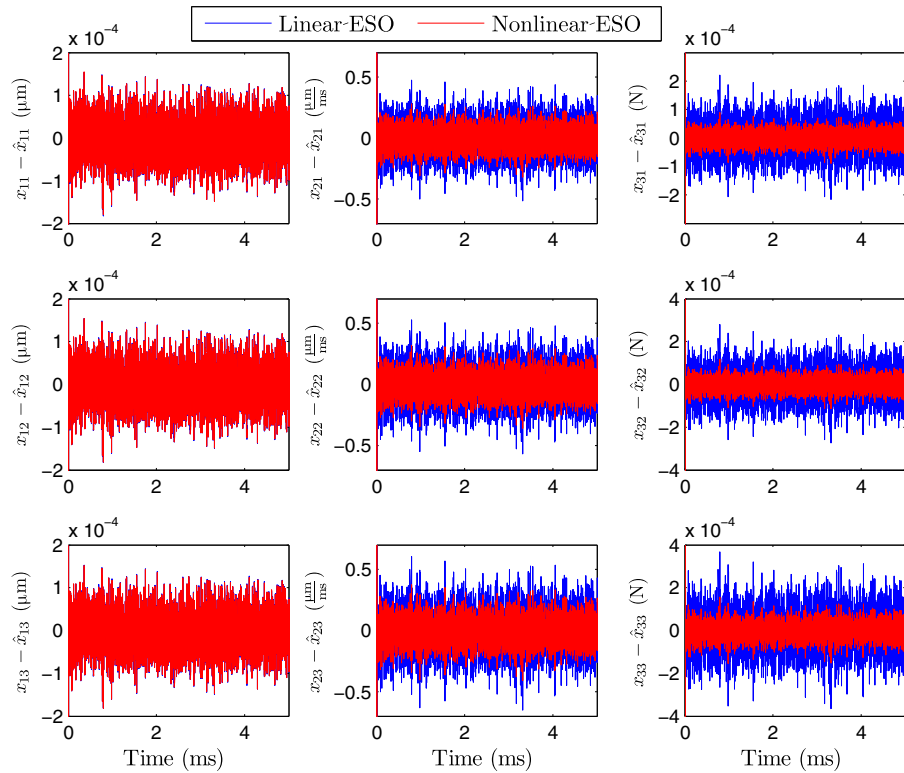


FIGURE 5 Comparison of the estimation errors of the linear and nonlinear extended state observers (ESOs) [Colour figure can be viewed at wileyonlinelibrary.com]

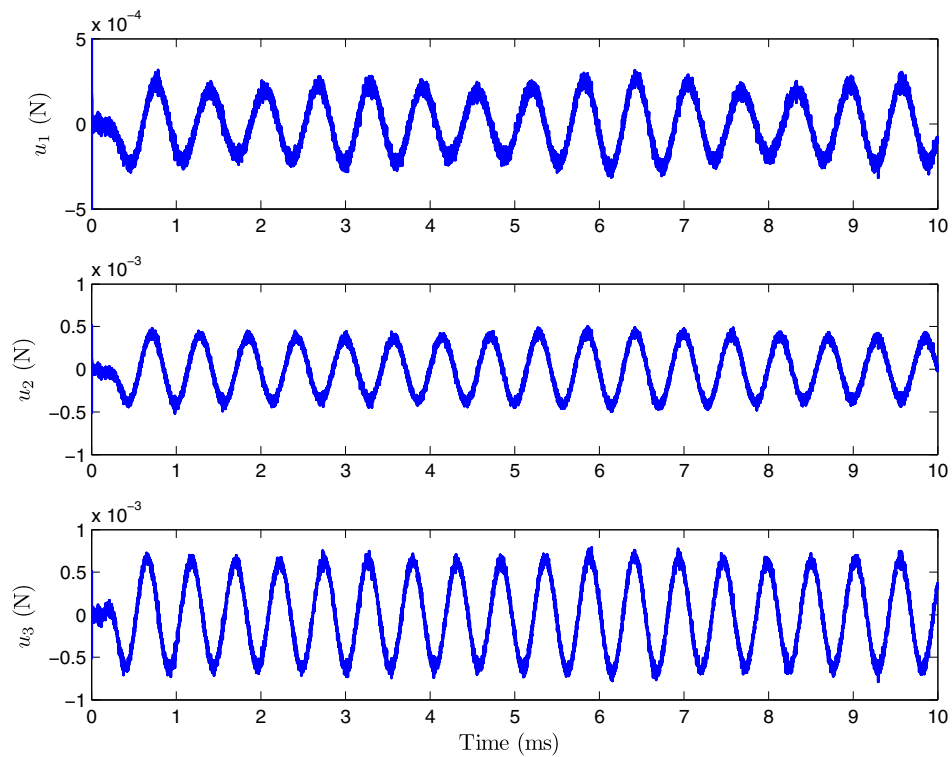


FIGURE 6 Control inputs u_1 , u_2 , and u_3 [Colour figure can be viewed at wileyonlinelibrary.com]

uses a high-gain linear ESO that estimates both states and internal dynamics of the gyroscope system. In the trajectory tracking loop, a high-gain proportional-derivative (PD) error feedback is used. The bandwidths of the linear ESO

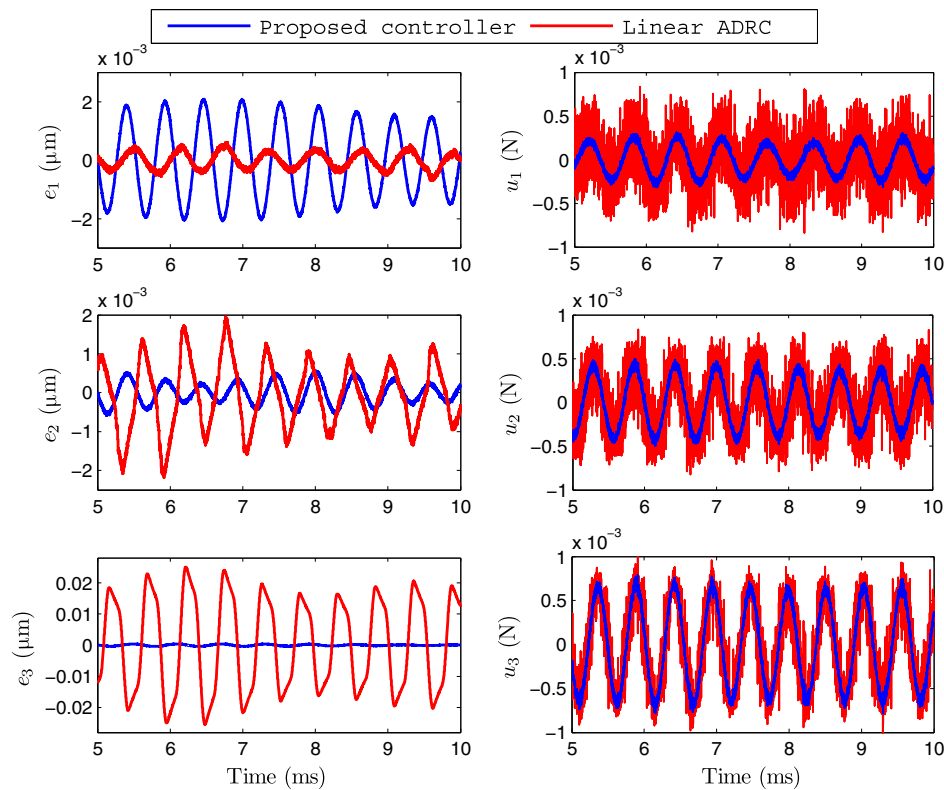


FIGURE 7 Comparison of the steady-state tracking errors and control signals of the proposed controller and the linear active disturbance rejection control (ADRC) [Colour figure can be viewed at wileyonlinelibrary.com]

and the PD controller are tuned as 5×10^3 and 10^3 , respectively (see the work of Zheng et al.⁷ for details). The comparison between the steady-state tracking errors and the control signals of the controllers is given in Figure 7. While the linear ADRC has a better tracking performance along the first vibration axis, in the other 2 axes, our proposed controller outperforms the linear ADRC and achieves much smaller tracking errors. Moreover, the control signals of linear ADRC exhibit a chattering-like behavior, and in the first 2 axes of the gyroscope, they have larger amplitudes compared with the proposed controller.

8 | CONCLUDING REMARKS

In this paper, we have proposed a new controller for the vibration control of a triaxial MEMS gyroscope through combining the active disturbance rejection and the output regulation methodologies. This control paradigm relaxes the need for accurate modeling of the sensor's vibration modes. A nonlinear ESO was used to cope with the disturbances without a known frequency spectrum. This method allowed us to apply an internal model-based output regulation control to the nominal gyroscope system. To further attenuate the effect of the ESO estimation errors, the energy-to-peak robust control technique was employed in the nominal output regulation. The ultimate boundedness of the closed-loop trajectories was investigated and proved in the framework of Lyapunov stability and the center manifold theory. Representative numerical simulations were presented to support the analytical results and to show the efficiency of the proposed control method. Estimation of the gyroscope parameters, including the input angular velocity, was not discussed in this paper. To estimate the gyroscope parameters, one can augment an outer parameter estimation loop with the control system. While the parameter estimator identifies the unknown parameters, the controller drives the mechanical energy of the gyroscope to a suitable level that guarantees the convergence of the parameter estimation. The parameter estimation algorithm can be designed using the optimization-based techniques such as the gradient or the least squares methods. The least squares parameter estimation method has been elaborated in our previous research work⁸ for a single-axis MEMS gyroscope. An extended parameter estimation algorithm for the case of the triaxial gyroscope will be pursued in future works.

ORCID

Jafar Keighobadi  <http://orcid.org/0000-0002-1216-4518>

REFERENCES

1. Yazdi N, Ayazi F, Najafi K. Micromachined inertial sensors. *Proc IEEE*. 1998;86(8):1640-1658.
2. Zhanshe G, Fucheng C, Boyu L, Le C, Chao L, Ke S. Research development of silicon MEMS gyroscopes: a review. *Micro Tech*. 2015;21(10):2053-2066.
3. Laermer F. Mechanical microsensors. In: Korvink JG, Paul O, eds. *MEMS: A Practical Guide to Design, Analysis, and Applications*. Berlin, Heidelberg: Springer; 2006:523-566.
4. Acar C, Shkel A. *MEMS Vibratory Gyroscopes: Structural Approaches to Improve Robustness*. Boston, MA: Springer; 2009.
5. Shkel AM, Horowitz R, Seshia AA, Park SPS, Howe RT. Dynamics and control of micromachined gyroscopes. Paper presented at: Proceedings of the 1999 American Control Conference (Cat. No. 99CH36251), Vol. 3; 1999; San Diego, CA, USA.
6. Park S, Horowitz R. New adaptive mode of operation for MEMS gyroscopes. *J Dyn Syst Meas Control*. 2005;126(4):800-810.
7. Zheng Q, Dong L, Lee DH, Gao Z. Active disturbance rejection control for MEMS gyroscopes. *IEEE Trans Control Sys Tech*. 2009;17(6):1432-1438.
8. Hosseini-Pishrobat M, Keighobadi J. Force-balancing model predictive control of MEMS vibratory gyroscope sensor. *Proc Inst Mech Eng Part C: J Mech Eng Sci*. 2016;230(17):3055-3065.
9. Barbour N, Schmidt G. Inertial sensor technology trends. *IEEE Sensors J*. 2001;1(4):332-339.
10. John JD, Vinay T. Novel concept of a single-mass adaptively controlled triaxial angular rate sensor. *IEEE Sensors J*. 2006;6(3):588-595.
11. Fei J, Zhou J. Robust adaptive control of MEMS triaxial gyroscope using fuzzy compensator. *IEEE Trans Syst Man Cybern Part B: Cybern*. 2012;42(6):1599-1607.
12. Song Z, Li H, Sun K. Adaptive dynamic surface control for MEMS triaxial gyroscope with nonlinear inputs. *Nonlinear Dyn*. 2014;78(1):173-182.
13. Han J. From PID to active disturbance rejection control. *IEEE Trans Ind Electron*. 2009;56(3):900-906.
14. Huang Y, Xue W. Active disturbance rejection control: methodology and theoretical analysis. *ISA Trans*. 2014;53(4):963-976.
15. Madoński R, Herman P. Survey on methods of increasing the efficiency of extended state disturbance observers. *ISA Trans*. 2015;56:18-27.
16. Huang J, Chen Z. A general framework for tackling the output regulation problem. *IEEE Trans Autom Control*. 2004;49(12):2203-2218.
17. Isidori A, Marconi L, Serrani A. Fundamentals of internal-model-based control theory. In: *Robust Autonomous Guidance: An Internal Model Approach*. London: Springer; 2003.
18. Chen Z, Huang J. Robust output regulation: a framework. In: *Stabilization and Regulation of Nonlinear Systems: A Robust and Adaptive Approach*. Cham, Switzerland: Springer; 2015.
19. Zhiyong CZ, Jie Huang J. Attitude tracking and disturbance rejection of rigid spacecraft by adaptive control. *IEEE Trans Autom Control*. 2009;54(3):600-605.
20. Chen Z, Huang J. Attitude tracking of rigid spacecraft subject to disturbances of unknown frequencies. *Int J Robust Nonlinear Control*. 2014;24(16):2231-2242.
21. Sun W, Lan J, Yeow JTW. Constraint adaptive output regulation of output feedback systems with application to electrostatic torsional micromirror. *Int J Robust Nonlinear Control*. 2013;25:504-520.
22. Zheng B, Zhong Y. Robust attitude regulation of a 3-DOF helicopter benchmark: theory and experiments. *IEEE Trans Ind Electron*. 2011;58(2):660-670.
23. Younis MI. *MEMS Linear and Nonlinear Statics and Dynamics, Microsystems*. Vol. 20. Boston, MA: Springer; 2011.
24. Gabrielson T. Mechanical-thermal noise in micromachined acoustic and vibration sensors. *IEEE Trans Electron Devices*. 1993;40(5):903-908.
25. Boser BE. Electronics for micromachined inertial sensors. Paper presented at: Proceedings of the International Solid State Sensors and Actuators Conference (Transducers '97), Vol. 2. IEEE; 1997; Chicago, IL, USA.
26. Chen Z, Xu D. Output regulation and active disturbance rejection control: unified formulation and comparison. *Asian J Control*. 2016;18(5):1668-1678.
27. Ball AA, Khalil HK. High-gain observers in the presence of measurement noise: a nonlinear gain approach. Paper presented at: 47th IEEE Conference on Decision and Control; 2008; Cancun, Mexico.
28. Sastry S. *Nonlinear Systems: Analysis, Stability, and Control*. Interdisciplinary Applied Mathematics. New York, NY: Springer; 1999.
29. Khalil HK. *Nonlinear Systems*. Pearson Education. 3rd ed. Upper Saddle River, NJ: Prentice Hall; 2002.
30. Boyd S, Ghaoui LE, Feron E, Balakrishnan V. *Linear Matrix Inequalities in System and Control Theory*. Studies in Applied Mathematics: Society for Industrial and Applied Mathematics; 1994; Philadelphia, PA.
31. Skelton RE, Iwasaki T, Grigoriadis KM. *A Unified Algebraic Approach to Linear Control Design*. London: Taylor & Francis; 1997.
32. Zhang H, Zhang X, Wang J. Robust gain-scheduling energy-to-peak control of vehicle lateral dynamics stabilisation. *Veh Syst Dyn*. 2014;52(3):309-340.

33. Kheloufi H, Zemouche A, Bedouhene F, Boutayeb M. On LMI conditions to design observer-based controllers for linear systems with parameter uncertainties. *Automatica*. 2013;49(12):3700-3704.
34. Grant M, Boyd S. CVX: Matlab Software for Disciplined Convex Programming, version 2.1. 2014. <http://cvxr.com/cvx>
35. Grant M, Boyd S. Graph implementations for nonsmooth convex programs. In: Blondel V, Boyd S, Kimura H, eds. *Recent Advances in Learning and Control*. Lecture Notes in Control and Information Sciences: Springer-Verlag Limited; 2008.

How to cite this article: Hosseini-Pishrobat M, Keighobadi J. Robust output regulation of a triaxial MEMS gyroscope via nonlinear active disturbance rejection. *Int J Robust Nonlinear Control*. 2018;28:1830–1851. <https://doi.org/10.1002/rnc.3983>